



Toward error-free scaled spin torque majority gates

Cite as: AIP Advances 6, 065304 (2016); <https://doi.org/10.1063/1.4953672>

Submitted: 17 November 2015 . Accepted: 27 May 2016 . Published Online: 06 June 2016

Adrien Vaysset, Mauricio Manfrini , Dmitri E. Nikonov , Sasikanth Manipatruni, Ian A. Young, Geoffrey Pourtois, Iuliana P. Radu, and Aaron Thean



View Online



Export Citation



CrossMark

ARTICLES YOU MAY BE INTERESTED IN

[Operating conditions and stability of spin torque majority gates: Analytical understanding and numerical evidence](#)

Journal of Applied Physics **121**, 043902 (2017); <https://doi.org/10.1063/1.4974472>

[Interconnected magnetic tunnel junctions for spin-logic applications](#)

AIP Advances **8**, 055921 (2018); <https://doi.org/10.1063/1.5007622>

[Non-volatile spin wave majority gate at the nanoscale](#)

AIP Advances **7**, 056020 (2017); <https://doi.org/10.1063/1.4975693>

AIP Conference Proceedings
FLASH WINTER SALE!

50% OFF ALL PRINT PROCEEDINGS

ENTER CODE 50DEC19 AT CHECKOUT



Toward error-free scaled spin torque majority gates

Adrien Vaysset,^{1,a} Mauricio Manfrini,¹ Dmitri E. Nikonov,²
 Sasikanth Manipatruni,² Ian A. Young,² Geoffrey Pourtois,¹ Iuliana P. Radu,¹
 and Aaron Thean¹

¹IMEC, Kapeldreef 75, 3001 Leuven, Belgium

²Exploratory Integrated Circuits, Components Research, Intel Corp., Hillsboro,
 Oregon 97124, USA

(Received 17 November 2015; accepted 27 May 2016; published online 6 June 2016)

The functionality of a cross-shaped Spin Torque Majority Gate is explored by means of micromagnetic simulations. The different input combinations are simulated varying material parameters, current density and size. The main failure mode is identified: above a critical size, a domain wall can be pinned at the center of the cross, preventing further propagation of the information. By simulating several phase diagrams, the key parameters are obtained and the operating condition is deduced. A simple relation between the domain wall width and the size of the Spin Torque Majority Gate determines the working range. Finally, a correlation is found between the energy landscape and the main failure mode. We demonstrate that a macrospin behavior ensures a reliable majority gate operation. © 2016 Author(s). All article content, except where otherwise noted, is licensed under a Creative Commons Attribution (CC BY) license (<http://creativecommons.org/licenses/by/4.0/>). [<http://dx.doi.org/10.1063/1.4953672>]

Continual miniaturization of Complementary Metal-Oxide-Semiconductor (CMOS) field effect transistors has been a great success in the past 40 years. However, scaling is now approaching fundamental limits.¹ In this regard, spintronics² could provide a new paradigm, taking advantage of its low power and non-volatility. A spin-polarized current can manipulate the magnetization of a ferromagnetic layer via the Spin Transfer Torque (STT) effect.^{3,4} This is used in STT-MRAM⁵ to switch the magnetic state. These memory devices can be combined with CMOS logic to build hybrid magnetic/CMOS architectures.⁶ In more drastic approaches, the ferromagnet is part of the logic circuit. For example, in Nano-Magnetic Logic,⁷⁻¹⁰ information propagates between nanoscale magnets via dipolar coupling. A logic gate can also be built with a Magnetic Tunnel Junction (MTJ) controlled either by an external magnetic field¹¹ or by STT and stray field.¹² Nevertheless, larger speed and higher density are expected if the signal is directly transmitted through a continuous free layer, as in Domain Wall (DW) logic.¹³⁻¹⁶

Most of these concepts implement the common NAND, NOR or NOT functions, while others^{8,9,17} utilize a majority gate. It is known that any arithmetic operation can be synthesized from inverters and three-input majority gates.¹⁸ Logic circuits based on such gates are expected to be more compact.

Thus, four features are essential for disruptive spin logic: (1) majority gate for more compact circuits, (2) low power spin manipulation, (3) continuous spintronic bus for potential high speed and high density, (4) bistable states for non-volatility. Even though a few technologies previously cited have several of these advantages, none of them meet these four criteria. In fact, only two concepts fulfill these conditions: the all-spin logic device¹⁹⁻²¹ and the Spin Torque Majority Gate (STMG).²² The former requires improvement of current material properties such as the spin diffusion length and spin injection efficiency, while the latter should benefit from materials already developed for MRAM stacks. Nikonov *et al.* introduced the concept of the STMG²² and studied variations of the free layer shape.²³ Here, we focus on the operating range of the conventional cross-shaped STMG, which is the most promising geometry explored so far.

^aAlso at Departement elektrotechniek (ESAT), KU Leuven, Leuven, Belgium

The STMG consists of an out-of-plane free layer shared by four MTJs. The logical state ('0' or '1') is encoded in the orientation of the free layer magnetization ('UP' or 'DOWN'). It is controlled by Current-Perpendicular-to-Plane (CPP) spin torque via the three input MTJs. The output magnetization state is detected by the fourth MTJ via the Tunnel Magnetoresistance. The STT is acting only at the inputs. In the rest of the free layer, the magnetization is mainly driven by the magnetic exchange interaction since no in-plane current is injected. As a consequence, the STMG can only work if the four MTJs are close enough to each other.

Magnetization dynamics is simulated in the free layer using the micromagnetic solver OOMMF.²⁴ The free layer thickness is $t = 1.2$ nm and the mesh cells are $2 \times 2 \times 1.2$ nm³. The anisotropy is set along the z -axis (out-of-plane). Like in Ref. 22, the current is assumed to flow along $\pm z$ in the square areas defined by the input MTJs. At the end of the current pulse, the magnetization relaxes towards the nearest equilibrium state. The Oersted field generated by the current is not taken into account.

Simulations were run varying the saturation magnetization M_s , the exchange constant A_{ex} , the anisotropy constant K_u (defined as the ratio of the surface anisotropy K_s over the thickness t), the arm width a , the current density J and the pulse duration. For each set of parameter values, the five input combinations shown in Fig. 1 were simulated. The initial state was chosen to be pointing UP, with small deviations with respect to the z -axis in order to initiate the switching. The amplitude of these deviations is of no importance as we do not focus on switching speed performance.²⁵ Similarly, we do not intend to predict the operating current, since it will depend, in reality, on the stack composition and the quality of the MTJs.

For the input combinations A and B (defined in Fig. 1), the final output state is expected to be UP, which is identical to the initial state. This behavior is confirmed by all the simulations that were performed. In fact, not only the output arm is UP, but the entire cross is pointing upward at the final stage.

The combinations C, D and E are more critical. As shown in figure 2, they work below a maximum size. An increase of this critical size is observed when the exchange constant A_{ex} is increased. This is expected since the switching of the output arm relies mainly on the exchange interaction.

The working conditions of the E and D configurations are not discussed in detail here. As seen on figure 2, the input combination C is the most critical because it requires a smaller size. This is confirmed by all the simulations that were performed. Therefore, in the remainder of this article, we shall focus on the operating condition of C. Its failure will be referred to as the "main failure mode".

Fig. 3 shows the final state of the 'C' configuration for two sizes and several current values. For an arm width $a = 10$ nm, the output switches successfully above the threshold current. However, at $a = 20$ nm, the main failure mode is observed. This magnetic state consists of a DW pinned at the center of the cross. It is formed during the pulse of current and remains stable afterward. Interestingly, this DW can be Bloch or Néel.²⁶ The cross shape creates magnetostatic surface charges for the two types of DW. This is in contrast with the common case of a strip where surface charges exist only for the Bloch DW. Consequently, here, the two configurations have about the same energy. Therefore, the pinning does not seem to depend on the type of DW.

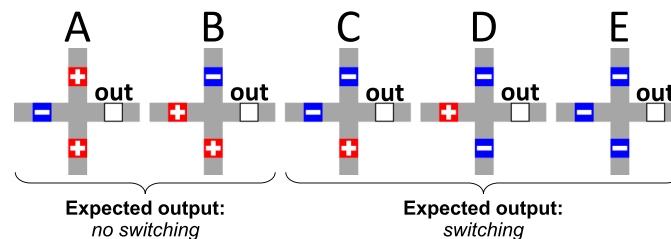


FIG. 1. Simulated input combinations. The symbols '+' and '-' represent the voltage polarities. In our convention, '+' pushes the magnetization up and '-' brings it down. Since the initial state is UP, a majority of '+' should leave the output unchanged (combinations 'A' and 'B'), while a majority of '-' should switch it (combinations 'C', 'D' and 'E').

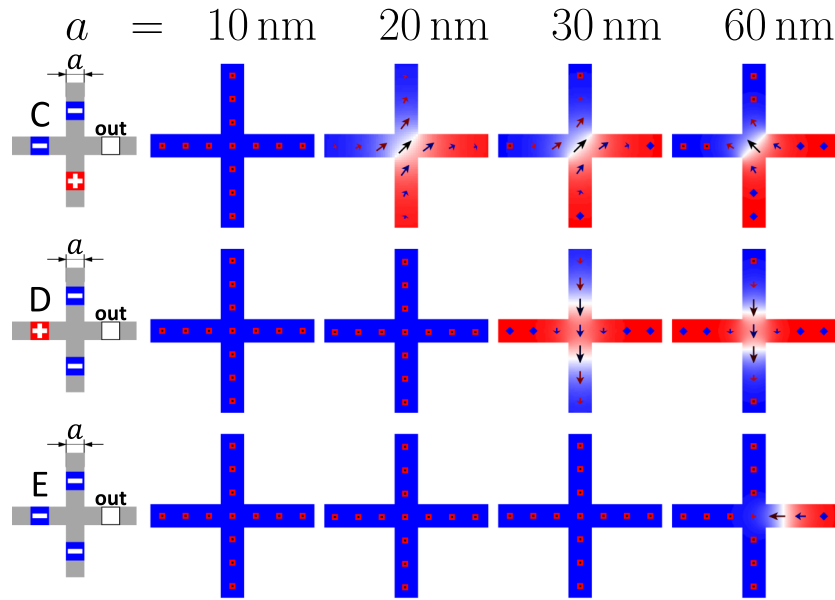


FIG. 2. Final states varying the arm width a for the input combinations C, D and E. Red: magnetization UP. Blue: magnetization DOWN. At $a = 10$ nm, the three configurations work (output in blue, i.e. switched), while at 60 nm, they all fail (output in red, i.e. unswitched). The C configuration is the one requiring the smallest size. Simulation parameters are $M_s = 800$ kA/m, $K_u = 400$ kJ/m³, $A_{ex} = 2 \times 10^{-11}$ J/m. The current density in the MTJs is above the threshold value.

For the sizes that work regardless of the combination, a seems to be smaller than the DW width. In such a small device, the magnetization is mainly driven by the exchange interaction, which means that the only equilibrium states are uniform. Therefore, the final state is always uniform. However, large spatial variations are observed when the current is applied. During the pulse, the spin torque causes magnetization motion in the input areas. Since the device is very small, this motion is transmitted to the entire free layer via the exchange interaction. A complicated reversal mechanism occurs.²⁶ At the end of the pulse, each input arm points in the direction induced by its input MTJ. The output arm follows the majority, due to minimization of the exchange energy. Then, the system relaxes to the closest equilibrium state which is uniform and points in the majority direction.

It is worth mentioning that above the switching current density J_c , the final state is either always successful, or always in the main failure state.

Each simulation parameter seems to influence the final output state. In order to find the operating conditions, the total parameter space must be reduced. Since we choose not to focus on performance, the pulse duration and amplitude can be set to large values ensuring that $J > J_c$.

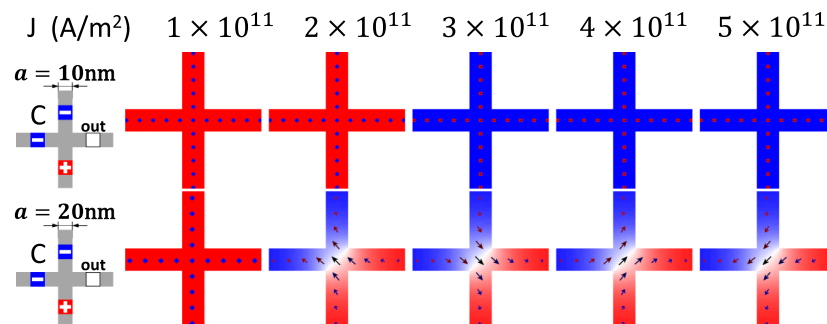


FIG. 3. Final micromagnetic states for the C configuration. Here, failure is observed from $a = 20$ nm. Input parameters are as in Fig. 2.

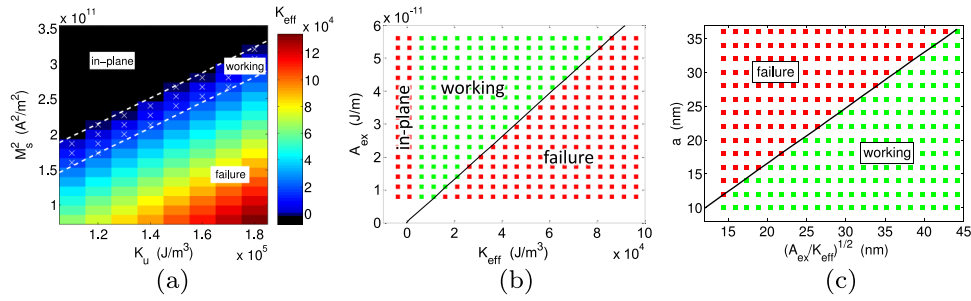


FIG. 4. STMG operating conditions. (a) K_u and M_s are varied, while $A_{ex} = 2 \times 10^{-11}$ J/m and the arm width is $a = 20$ nm. The color represents K_{eff} . Successful majority operation is determined by a limit value of K_{eff} . (b) Phase diagram varying A_{ex} and K_{eff} . The successful condition is given by a critical value of A_{ex}/K_{eff} . (c) Phase diagram where a and $\sqrt{A_{ex}/K_{eff}}$ are both varied. A straight line separates failure and success.

In a perpendicular free layer, the anisotropy constant is

$$K_{eff} = K_u - \frac{1}{2} \mu_0 M_s^2 (N_{zz} - N_{xx}) \quad (1)$$

where N_{xx} and N_{zz} are the demagnetizing coefficients. Fig. 4(a) illustrates this simple relation. K_{eff} shown in this figure is calculated according to the definition $K_{eff} = \mu_0 M_s (H_{demag} + H_{anis})/2$, where H_{demag} is the demagnetizing field and H_{anis} is the anisotropy field in a perpendicularly saturated state. Since H_{eff} varies spatially, we extracted its average over the free layer. Moreover, Fig. 4(a) shows that, for constant arm width $a = 20$ nm and constant exchange parameter $A_{ex} = 2 \times 10^{-11}$ J/m, the working range is only determined by K_{eff} , more specifically $0 < K_{eff} < 34$ kJ/m³. Therefore, K_{eff} is a key parameter for operation conditions.

Figure 4(b) represents a new series of simulations where A_{ex} and K_{eff} are both varied.²⁶ The arm width a is still 20 nm. Simulations exhibiting the majority gate behavior are shown in green. As expected, the in-plane state is obtained when $K_{eff} \leq 0$. For positive K_{eff} , the working range is delimited by A_{ex}/K_{eff} , which is a key parameter of the system.

Lastly, the arm width is varied, as shown in Fig. 4(c). The DW remains pinned at the center of the cross if $\sqrt{A_{ex}/K_{eff}} < 1.21 a$. Since 'C' is the most restrictive input combination, we conclude that the operating condition of the STMG is

$$\sqrt{\frac{A_{ex}}{K_{eff}}} > 1.21 a. \quad (2)$$

The parameter $\sqrt{A_{ex}/K_{eff}}$ is known as the Bloch length and is proportional to the DW width. Therefore, the DW stability is determined by the ratio of its width and the size of the device.

Note that there is no in-plane current. The out-of-plane current is localized in the MTJs, pushing the DW via the exchange interaction. Its effect seems negligible when the DW reaches the center of the cross. Therefore, we infer that the DW remains at the center if this is an energy minimum and that the failure disappears when it becomes a saddle point of the energy landscape. To verify this, more simulations are performed: starting from the failure state, the system relaxes to the nearest energy minimum. These final equilibrium states are shown in Fig. 5(a) ("equilibrium simulations"). They are compared to STT simulations in which the current density $J > J_c$ flows in the inputs MTJs (Fig. 5(b)). In the region '1', the DW is an equilibrium state, which leads to failure. In the region '2', near $K_{eff} = 0$, the DW is unstable, leading to success. The comparison of the two phase diagrams proves that the STMG works if the DW is energetically unstable. However, the operating region is slightly wider in the STT simulations. The additional successful states correspond to a third case ('3') where the DW is in a shallow energy well (Fig. 5(e)). In this situation, the STMG is very sensitive to initial conditions. Depending on the exact magnetization trajectory, the system may end up either in the DW state or in the uniform configuration. In a more realistic model, thermal fluctuations (not included here) should help overcome a shallow energy well.

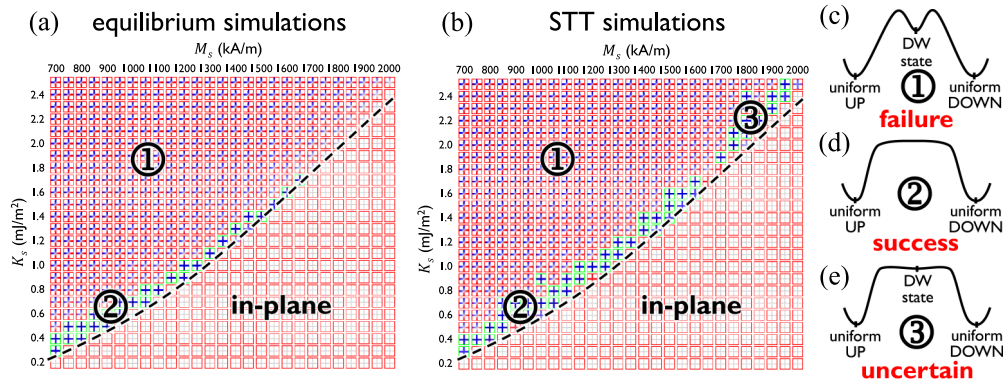


FIG. 5. (a) Final states of simulations without current, starting from an initial DW state. The magnetic state has a red frame if the DW is stable or if the magnetization is in-plane (failed). The frame is green for unstable DW (successful). (b) Final states of simulations with STT. States with expected output are framed in green. Here, $a = 10$ nm, $A_{ex} = 3 \times 10^{-11}$ J/m. The plots (c), (d) and (e) are schematic representations of the energy as a function of the position of the wall. If the center is in a minimum, the DW is an equilibrium state. In the region '1' of the phase diagram, the DW is stable. It is therefore an energy minimum. In the region '2', it is unstable, suggesting that it corresponds to a saddle point. The region '3' is characterized by a shallow energy well for a DW at the center.

Consequently, the operating condition is determined by the energy landscape²⁷: the STMG works if the central DW is in a saddle point (region '2') or if it is in a very shallow energy well (region '3').

The case of a shallow energy well has been studied with more thorough simulations. A different final state can be observed when the initial condition is changed. Adding the Oersted field leads to a similar result: by slightly modifying the precession trajectory, the final state can be changed. Therefore, correct operation is really ensured when the only two energy minima are the uniform states (region '2'). Thermal fluctuations should widen the operating range by destabilizing the DW in a shallow well. However, such a study is beyond the scope of this letter.

In conclusion, the operating range of the STMG has been explored via micromagnetic simulations. After an extensive study including all the possible input combinations, a main failure mode has been identified. It consists of a DW pinned at the center of the cross. It has been found that the device is functional below a critical size determined by the DW instability. Varying the simulation parameters, the operating condition $\sqrt{A_{ex}/K_{eff}} > 1.21 a$ has been obtained. The link with the energy landscape has then been established: if the central DW is in an energy minimum, it is likely to remain there and cause failure. Therefore, the maximum functional size is given by the macrospin limit.

- ¹ V. Zhirnov, R. Cavin, J. Hutchby, and G. Bourianoff, *Proceedings of the IEEE* **91**, 1934 (2003).
- ² I. Žutić, J. Fabian, and S. D. Sarma, *Reviews of Modern Physics* **76**, 323 (2004).
- ³ L. Berger, *Physical Review B* **54**, 9353 (1996).
- ⁴ J. Slonczewski, *Journal of Magnetism and Magnetic Materials* **159**, L1 (1996).
- ⁵ C. Chappert, A. Fert, and F. N. Van Dau, *Nature Materials* **6**, 813 (2007).
- ⁶ G. Prenat, B. Dieny, M. El Baraji, V. Javerliac, and J.-P. Nozieres, *IEEE Transactions on Magnetics* **45**, 3400 (2009).
- ⁷ R. P. Cowburn and M. E. Welland, *Science* **287**, 1466 (2000).
- ⁸ S. Breitkreutz, J. Kiermaier, I. Eichwald, X. Ju, G. Csaba, D. Schmitt-Landsiedel, and M. Becherer, *IEEE Transactions on Magnetics* **48**, 4336 (2012).
- ⁹ I. Eichwald, S. Breitkreutz, G. Ziemys, G. Csaba, W. Porod, and M. Becherer, *Nanotechnology* **25**, 335202 (2014).
- ¹⁰ M. T. Niemier, E. Varga, G. H. Bernstein, W. Porod, M. T. Alam, A. Dingler, A. Orlov, and X. S. Hu, *IEEE Transactions on Nanotechnology* **11**, 220 (2012).
- ¹¹ A. Ney, C. Pampuch, R. Koch, and K. H. Ploog, *Nature* **425**, 485 (2003).
- ¹² L. Leem and J. S. Harris, *Journal of Applied Physics* **105**, 07D102 (2009).
- ¹³ D. A. Allwood, G. Xiong, C. C. Faulkner, D. Atkinson, D. Petit, and R. P. Cowburn, *Science* **309**, 1688 (2005).
- ¹⁴ D. M. Bromberg, D. H. Morris, L. Pileggi, and J. G. Zhu, *IEEE Transactions on Magnetics* **48**, 3215 (2012).
- ¹⁵ J. A. Currihan, Y. Jang, M. D. Mascaró, M. A. Baldo, and C. A. Ross, *IEEE Magnetics Letters* **3**, 3 (2012).
- ¹⁶ K. Omari and T. Hayward, *Physical Review Applied* **2**, 044001 (2014).
- ¹⁷ S. Klingler, P. Pirro, T. Brächer, B. Leven, B. Hillebrands, and A. V. Chumak, *Applied Physics Letters* **105**, 152410 (2014).
- ¹⁸ S. B. Akers, in *3rd Annual Symposium on Switching Circuit Theory and Logical Design (SWCT 1962)* (IEEE, 1962), pp. 149–158.

- ¹⁹ B. Behin-Aein, D. Datta, S. Salahuddin, and S. Datta, *Nature Nanotechnology* **5**, 266 (2010).
- ²⁰ B. Behin-Aein, A. Sarkar, S. Srinivasan, and S. Datta, *Applied Physics Letters* **98**, 123510 (2011).
- ²¹ S. Manipatruni, D. Nikonov, and I. Young, [arXiv:1212.3362](https://arxiv.org/abs/1212.3362) (2012).
- ²² D. E. Nikonov, G. I. Bourianoff, and T. Ghani, *IEEE Electron Device Letters* **32**, 1128 (2011).
- ²³ D. E. Nikonov, S. Manipatruni, and I. A. Young, *Journal of Applied Physics* **115**, 24 (2014).
- ²⁴ M. Donahue and D. Porter, OOMMF User's Guide, Version 1.0, Interagency Report NISTIR 6376 (National Institute of Standards and Technology, Gaithersburg, MD, 1999).
- ²⁵ J. Z. Sun, *Physical Review B* **62**, 570 (2000).
- ²⁶ See supplementary material at <http://dx.doi.org/10.1063/1.4953672> for the simulation protocol of Figs 4 and for more details on the magnetization dynamics.
- ²⁷ Contrary to previous STT simulations, the boundary between success and failure is not a well-defined line. This difference is due to the current being just above its critical value instead of being much larger.